International Journal of Innovative Technology and Exploring Engineering (IJITEE)
ISSN: 2278-3075 (Online), Volume-9 Issue-2, December 2019

Moving Surface Boundary Layer Technique For NACA 0012 Airfoil At Ultra-Low Reynolds Number

Y. Joshi, A. Kumar, A. Roy, A. B. Harichandan

Abstract*: *Application of moving surface boundary layer control technique has been confined to relatively high Reynolds numbers. The present paper reports a numerical study of application of the above flow technique in the ultra-low Reynolds number range. A two dimensional incompressible unstructured grid based Navier Stokes solver has been used for conducting the numerical studies. Moving surface has been applied at three different portions on the airfoil surface, firstly, in the form of a rotating leading edge portion of the airfoil, secondly, a continuous moving surface from leading edge of airfoil to 57% of the chord along the leeward surface of the airfoil and thirdly a continuous moving surface from leading edge to 97% of the chord along the leeward surface of the airfoil. All the moving surface configurations show improvement of aerodynamic performance of the airfoil through enhancement of lift and decrement of drag as compared to a fixed surface one.

Keywords: Moving Surface Airfoil, Boundary Layer Control, Lift Enhancement, Drag Reduction, Aerodynamic Performance Enhancement, Ultra-Low Reynolds Number

I. INTRODUCTION

As the advent of Prandtl's boundary layer theory, there has been a constant interest to minimize its adverse effects. Different processes like vortex generators, suction, blowing etc. are analysed and are implemented on various geometries including aerodynamic shapes and bluff bodies. Using a moving wall for controlling boundary layer has also been explored by several researchers during the last few decades. The authors strongly feel that this technique needs renewed attention in the context of modern day low Reynolds number applications. In all the above boundary layer control techniques, the primary motive of the control mechanism for delaying or preventing boundary layer separation. The word 'ultra-low' used in the title of the paper has been used to represent a Reynolds number range varying between a few hundred to around one thousand.

Revised Manuscript Received on January 30, 2020.
***** Correspondence Author
Y. Joshi, Department of Mechanical Engineering, Marwadi University, Rajkot,Gujrat,India.
Ankit kumar, Department of Aerospace Engineering, KIIT (DU), Bhubaneswar, India.
A. Roy, Department of Aerospace Engineering, IIT Kharagpur, West Bengal, India.
Atal Bihari Harichandan*, Department of Aerospace Engineering, KIIT (DU), Bhubaneswar, India.

At these Reynolds numbers the flow is very strongly dominated by thick viscous layers developing on the body surface. The boundary layer is not robust and is accessible to separation even under weak adverse pressure gradient. The present work investigates the effectiveness of a moving boundary in controlling or minimising the adverse effect of large scale separation of flow from the surface of airfoil in the presence of such thick viscous layers. Johnson et al. [1] studied the concept of using a leading edge rotating cylinder on an airfoil to control its lift. Mokhtarian and Modi [2] have used a potential flow model to study the effects of leading edge rotating cylinder happening flow past Joukowsky airfoil. Modi and Mokhtarian [3] have experimentally examined the effect of moving surface boundary layer (MSBL) control intended for flow past a Joukowsky airfoil with rotating cylinders situated at leading and trailing-edge. Hassan and Sankar [4] have numerically investigated the effect of rotation of leading edge on flow over various airfoils including NACA 0012. Kubo et al. [5] have studied the aspect of aerodynamic instability phenomena using MSBL control. Modi et al. [6] numerically and experimentally investigated the effect of rotating leading-edge, trailing-edge, upper leading-edge, forward upper-surface and rear upper-surface cylinder on the flow characteristics of a Joukowsky airfoil. A very extensive analysis on MSBL control technique with its proper utilizations is found in Modi [7]. Azuma and Nakamura [8] have numerically investigated the flow past a 45^0 swept delta wing with a rotating leading edge. All the above investigations have been performed at fairly high Reynolds numbers varying from 10^4-10^6 based on the airfoil chord.

In the first part of the paper numerical simulations performed for two different problems, firstly, flow past NACA 0012 airfoil without moving surface at Reynolds number (*Re*) = 1200 and secondly flow over a rotating circular cylinder undergoing translation at *Re* ranging from 20 to 100 are reported. The above numerical simulations are perfumed to establish the capability of the Navier Stokes solver 'CFRUNS' (Harichandan and Roy [9]) to study flow past airfoil and moving surface geometries at ultra-low Reynolds number. In the second part of the paper simulations are performed for uniform flow impinging on an airfoil with a moving surface. The moving surface is simulated by specifying a non-zero tangential velocity on the airfoil surface as a boundary condition. This boundary condition is suitably applied over different parts of airfoil surface to simulate different test cases.

The prescription of net zero normal velocity on the airfoil surface is automatically ensured and therefore the airfoil's shape is not affected by the moving boundary condition. The moving airfoil surface energises the boundary layer developing on it through injection of tangential momentum. This is called as 'Moving Surface Boundary Layer Control' strategy by means of which aerodynamic performance of a shape can be improved by increasing lift, lift to drag ratio, decreasing drag etc. and therefore making it more aerodynamically efficient. This technique has been applied for the past few decades on various configurations including airfoils, wings and bluff bodies, but all such studies were conducted at much higher Reynolds numbers as mentioned before. The low Reynolds number world is unfolding with its miriad applications in recent times. The present paper attempts to address the issue of effectiveness of this flow control technique at ultra-low Reynolds numbers. This may help explore its possible applications in micro flow control devices, micro air vehicle aerodynamic control etc.

In the present study, the moving surface has been considered at three different locations on airfoil surface as follows:

(a) Rotating leading edge.

(b) Moving surface from leading edge to 57% of the chord along the leeward surface of the airfoil.

Moving surface from leading edge to 97% of the chord along the leeward surface of the airfoil.

Location of the above moving surfaces are shown schematically in Figure 1 below:

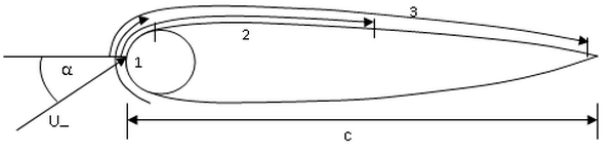

Figure 1. Location of moving surface on airfoil.

The aerodynamic performance of the above three flow control cases is compared with that of fixed surface airfoil in order to assess the merit of the technique at ultra-low Reynolds number. In an actual configuration the moving surface of the airfoil may be simulated by having a belt supported by adequate number of rotating micro rollers located at close gaps below the surface at various locations in order to maintain the airfoil profile with high fidelity.

II. GOVERNING EQUATIONS AND MATHEMATICAL SCHEME

Governing equations for 2-d incompressible viscous flows devoid of heat transfer and body forces effects are written in non-dimensional form using indicial notations follows:

Continuity Equation
$$\frac{\partial u_i}{\partial x_i} = 0 \qquad (1)$$

Momentum Equations
$$\frac{\partial u}{\partial t} + \frac{\partial}{\partial x_j}\left(u_j u_i\right) = -\frac{\partial p}{\partial x_i} + \frac{\partial \tau_{ij}}{\partial x_j} \qquad (2)$$

The above equations have been used in non-dimensional form for present computations. The equations have been non-dimensionalized in consideration of '*c*','d', 'U_∞' which represent chord of the airfoil, cylinder diameter and free stream velocity respectively. In present analysis, the value of velocity and pressure at free-stream is assumed as initial value for every computational cell. The governing equations are discretized and computed using a finite volume scheme on rectangular computational domain. Accuracy of the spatial and temporal terms in the numerical scheme is second order. The temporal terms are discretized by a second order accurate Adams-Bashforth scheme. Spatial terms are discretized using second order accurate central differencing scheme. Dirichlet boundary condition of free- stream velocity is maintained at inlet and zero normal velocity gradient is maintained at outlet, top and bottom boundaries. Zero pressure gradient is considered at inlet, top and bottom boundaries as well as on the body surface in normal direction. Free-stream pressure is assigned at outlet boundary. The upstream boundary is situated at *5c* from the airfoil mid chord and the zero shear top and the bottom boundaries are both situated at a distance *10c*. The outlet boundary is situated at *30c* distance from mid chord of the airfoil. The boundary conditions have been modified in comparison with those used in Harichandan and Roy [9] in order to simulate results of comparable accuracy with smaller domain size. The pressure velocity coupling is achieved by computing a pressure Poisson equation. The fluxes at the cell face centers are reconstructed based on a procedure elaborated in Harichandan and Roy [9]. No slip boundary condition is applied on body surface. For moving surface, tangential surface velocity is non-zero and normal surface velocity is zero whereas on fixed body surface the velocity is set to zero. Additional details on the solver are reported in Harichandan and Roy [9, 10] and Roy and Bandyopadhyay [11].

Grid independence study was carried out for the numerical scheme and the results are shown in the Table 1.

Table 1. Grid Independence study at *Re* = 100.

Grid size (Grid no.)	Coefficient of drag (C_D)	Coefficient of lift (C_L)	Strouhal number (St)
80 (1)	1.112 ± 0.02101	± 0.1811	0.16801
120 (2)	1.185 ± 0.0151	± 0.2101	0.1641
160 (3)	1.352 ± 0.0101	± 0.2781	0.1611
200 (4)	1.358 ± 0.0101	± 0.2811	0.1611

Based upon the values of coefficient of lift, coefficient of drag and Strouhal number variation, grid 3 has been preferred for the flow calculation. For the same problem the above mentioned parameters of the present solver were compared with works of other researchers as mentioned in Table 2 below:

Table 2. : Parameters of flow field around the circular cylinder at *Re* = 100

Parameters	C_D	C_L	St
Ding et al. [12]	1.356 ± 0.010	± 0.287	0.166
Meneghini et al. [13]	1.370 ± 0.010	---	0.165

Braza et al. [14]	1.364 ± 0.015	± 0.25	0.160
Tritton [15]	1.320 ± 0.010	---	0.160
Wiesenberger [16]	1.326 ± 0.010	---	0.1608
Present	1.352 ± 0.010	± 0.278	0.161

In order to compare the capability of the solver in accurately matching with analytical result, it was used to compute Couette flow. The time dependent convergence of the solution to the analytical one was found to be satisfactory.

III. RESULTS AND DISCUSSION

A. Flow past a NACA0012 airfoil at Re = 1200

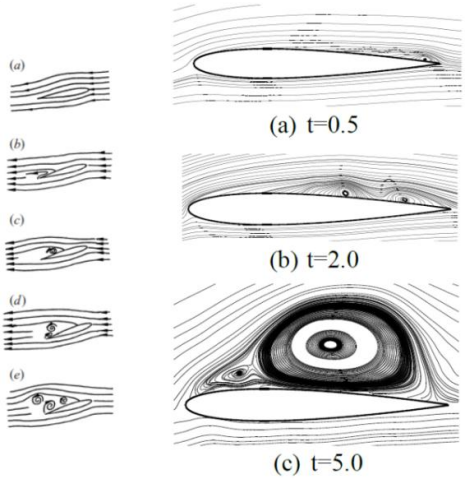

Figure 2. Schematic view of 'Separation Vortex' on the left and computed streamlines for *Re* = 1200, *α* = 15° at various time instants.

The streamlines past a NACA 0012 airfoil at *Re* = 1200, α = 15° at various instants of time computed using 'CFRUNS' scheme are shown in Figures 2(a) - 2(c) respectively. The flow corresponds to 'Type C: Separation Vortex' reported by Huang et al. [17]. Development of this flow pattern with time is elaborately explained in the above reference and schematically shown on the left side of Figure 2.

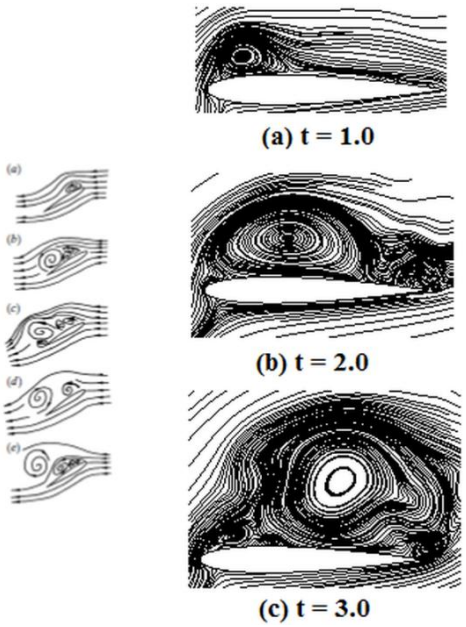

Figure 3. Schematic view of 'Leading Edge Vortex' on the left and computed streamlines for *Re* = 1200, *α* = 30° at various time instants.

The computed streamlines show emergence of a tiny separation bubble at the trailing edge at $t = 0.5$, where 't' is assigned as the non-dimensional time expressed as a ratio of the length scale 'c' and velocity scale 'U_∞'. The separation point gradually moves upstream as time evolves forming pockets of separation close to trailing edge which is followed by development of a separation bubble on leeward side which consequently leads to formation of a wake which is confined more in direction of trailing edge.

However, the evolution of separated flow structure on airfoil NACA 0012 at *Re* = 1200, α = 30° at different instants of time from the start of the flow are provided in Figure 3. The computed flow pattern is compared with flow visualization of Huang et al. [17]. For comparison, the different phases involved in the 'Type D: Leading Edge Vortex' mode as captured in the present numerical simulation are provided below along with the characteristics of this mode as explained in Huang et al. [17] and shown on left side of the figure. At $t = 1.0$ a fairly strong leading edge vortex is visible. At $t = 2.0$ the leading edge vortex grows stronger and covers almost two third of the leeward surface of the airfoil with finer eddy structures visible near the trailing edge. At $t = 3.0$ the large leeward side vortex deforms under the influence of a newly emerging vortex near leading edge and trailing edge vortex which is being shed. The large vortex is also on the verge of separating from the body surface. At later time the large vortex structure is shed from the leeward side and leads to formation of Karman vortex sheet in wake of the airfoil.

B. Flow past rotating cylinder undergoing translation

The performance of the 'CFRUNS' solver was tested for a moving boundary problem before applying it for the study of moving surface airfoil. Flow past a cylinder which is rotating undergoes translation at low *Re* number was computed using the solver. The established trend of almost linear increase in lift force with the increase in rotational speed ($\dot{\theta}$) was found. Table 3 shows the comparison of rate of increase of C_L with rotational speed at different Reynolds numbers between present results and those reported by Ingham et al. [18]. The comparison was found to be satisfactory. More studies on rotating and rotationally oscillating cylinder using 'CFRUNS' solver are reported in Supradeepan and Roy [19].

Table 3. Comparison of $dC_L/d\dot{\theta}$ for flow past a rotating cylinder under translation

$dC_L/d\dot{\theta}$	Ingham et. al [18]	Present result
Re = 20	~2.3	2.33
Re = 60	~2.4	2.45
Re = 100	~2.5	2.55

C. Flow past NACA0012 airfoil with moving surface

In this section results are discussed related to various aspects of aerodynamic behavior of NACA 0012 airfoil with moving surface compared with airfoil with fixed surface. The study includes time history and time-averaged lift and drags coefficients, surface shear stress,

surface pressure distribution, streamline patterns, boundary layer velocity distribution at various locations etc. The study is intended towards gaining greater understanding of the aerodynamic behavior of this airfoil at ultra-low Reynolds numbers. For the following test cases reported in this paper it is assumed that the velocity with which the moving surface translates is four times that of the free stream speed. In order to perform these simulations a grid independent study was done for fixed surface airfoil at *Re* = 100, α = 10° for three different grids with total number of cells ranging from 25000 to 40000 approximately. The finest grid of 40000 cells with 300 nodes on airfoil surface, was chosen for all remaining simulations reported in this paper.

C.1. Rotating leading edge

A typical time history of lift-drag for the airfoil NACA 0012 with rotating leading edge at *Re* = 100 and α = 10° is shown in Figure 4. From the figure, it could be noticed that lift and drag coefficient values asymptotically converge towards steady state at this angle of attack. However, at higher angles of attack, flow separates from the airfoil's leeward surface in spite of the momentum injection in boundary layer near leading edge through the rotating cylinder. This is reflected through lift and the drag time history for *Re* = 100, α = 30° shown in Figure 5.

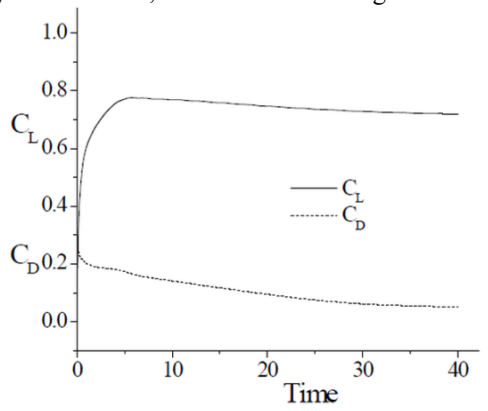

Figure 4. Time history of lift and drag coefficients for *Re* = 100, α = 10°

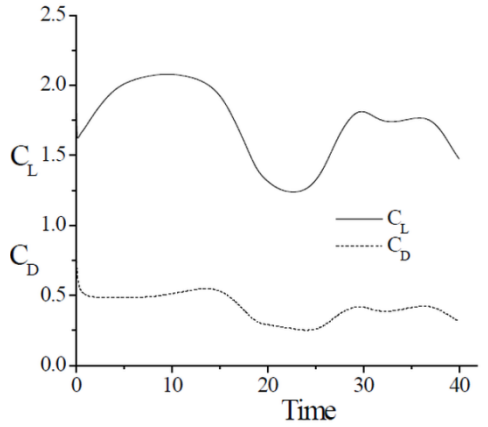

Figure 5. Time history of lift and drag coefficients for *Re* = 100, α = 30°

Figure 6 shows the distribution of entire velocity in flow field for *Re* = 100, α = 20°, *t* = 40. It is seen that higher values of total velocity are induced in the flow field near leading edge of airfoil due to rotation.

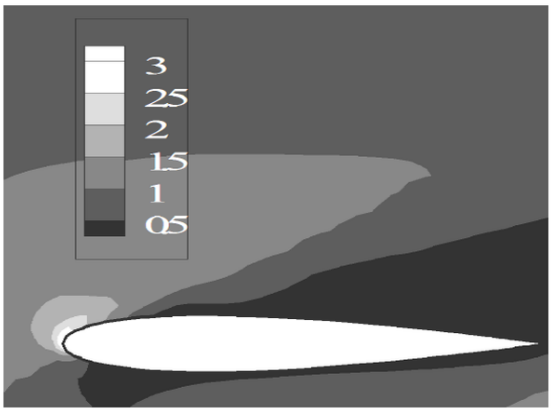

Figure 6. Total velocity field for *Re* = 100, α = 20°, *t* = 40

The time-averaged surface pressure distribution on airfoil is shown in the Figure 7. It is observed that due to the rotating cylinder a very strong suction peak is generated near the leading edge of the airfoil. Also, the enclosed area between the windward and leeward surface pressure of the airfoil keeps increasing up to α = 30° which indicates that the airfoil continues to generate lift effectively at that high angle of attack.

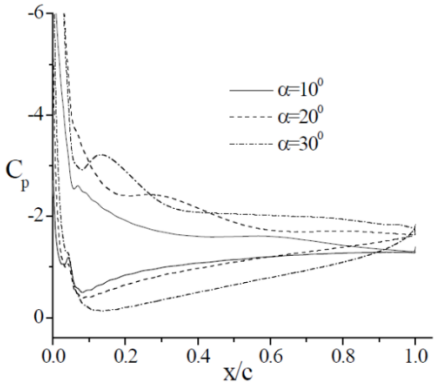

Figure 7. Time-averaged pressure distribution on the airfoil surface

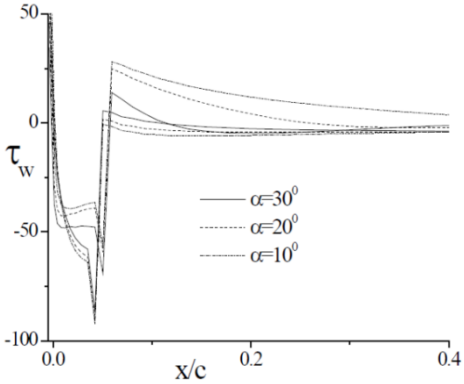

Figure 8. Time-averaged wall shear stress over the airfoil surface

Time-averaged wall shear stress distribution is shown in Figure 8. The figure shows that in region between the leading edge and approximately 0.05 - 0.07 x/c the wall shear stress first drops rapidly to large negative values followed by a sharp recovery to a positive peak. Beyond the positive peak the wall shear again decays gradually.

The maximum positive peak is achieved for α = 10° and it reduces with the increase in angles of attack. It is to be noted that flow separates over fast rotating cylinder surface which is indicated by the negative value of wall shear. However, it gains a large amount of tangential momentum due to strong shear produced by the rotating cylinder which helps to maintain the flow attached to the leeward surface of the airfoil at higher angles of attack. The high tangential momentum content leads to larger cross stream velocity derivative and therefore larger value of wall shear downstream beyond the rotating cylinder.

C.2. Moving surface from leading edge to 57% of the chord along the leeward surface of the airfoil

Instantaneous streamlines for this case are shown for various angles of attack in Figure 9 at t = 40. All these flows achieve steady state. It is seen that up to angles of attack of 30° there is negative evidence of large flow separation from the airfoil surface. With the increase in angles of attack the stagnation point moves towards the windward side of airfoil and the streamlines get highly clustered near the leading edge indicating increased flow acceleration in that region. This leads to formation of a very high suction peak which contributes towards lift enhancement. The attached flow also keeps the profile drag low

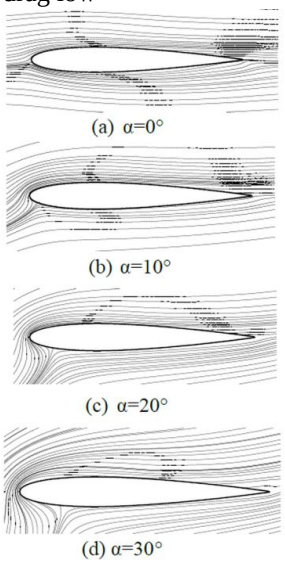

Figure 9. Instantaneous streamlines for *Re* = 100 and α = 0°30°

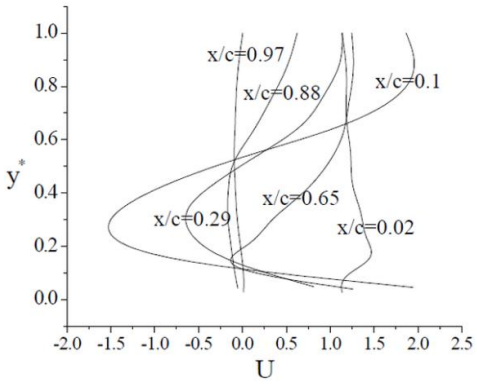

Figure 10. The time averaged boundary layer velocity profiles at different x/c stations for *Re* = 100, α = 40°

Nature of the time averaged boundary layer at different locations on airfoil surface for Re = 100, α = 40° is shown in Figure 10. It is observed that close to the airfoil's leading edge at (x/c) = 0.02, velocity maintains a fairly constant value with a peak of around 1.5 times free stream value. Beyond this station, strong inflection in the velocity profile and reverse flow is observed for stations ranging from (x/c) = 0.10 to 0.65 because of the large angle of attack. However, large values of velocity are observed near to the wall as well as the outer regions of the boundary layer for all these stations due to effect of the moving boundary. At the last two stations, namely (x/c) = 0.88 and 0.97, the velocity profiles are flatter and weak even near to the wall, because of absence of moving boundary in the aft portion of the leeward surface of the airfoil and due to strong flow separation in this region. It is to be noted that at each station on an average 20 cells within the boundary layer have been used to obtain the tangential velocity distribution. The normal distance from the wall is expressed in the form of a non-dimensional coordinate y*.

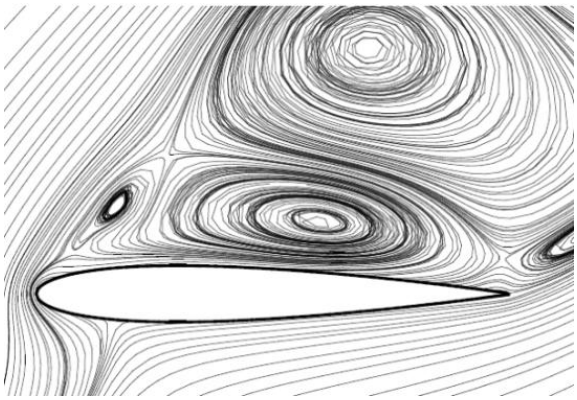

Figure 11. Instantaneous streamlines for *Re* = 100, α = 40° at *t* = 90

The instantaneous streamlines at t = 90 for Re = 100, α = 40° are shown in Figure 11. It is found that a fairly strong and stable vortex structure is attached to the leeward side of the airfoil. The moving boundary energizes the leeward surface flow which in turn assists the airfoil to generate modest amount of lift even at this large angle of attack. However, bluffness of the airfoil is enhanced due to large angle of attack and consequently drag acting on the airfoil is quite large. This leads to a nominal lift to drag ratio of order of one. See Figure 14 and 15 for lift and drag coefficient distribution as function of angle of attack. At lower angles of attack substantially better performance of the airfoil can be achieved as is already evident from the flow field features shown in Figure 9.

C.3. Moving surface from leading edge to 97% of the chord along the leeward surface of the airfoil

Time averaged boundary layer velocity profile at (x/c) = 0.1 and 0.65 for the various moving boundary and fixed surface airfoil cases are shown for α = 10° and 30° in Figures 12(a) and 12(b) respectively. Performance of four different configurations, namely (a) fixed surface airfoil (b) airfoil with rotating leading edge (c) moving surface from leading edge to 57% of the chord along the leeward surface of the airfoil (d) moving surface from leading edge to 97% of the chord along the leeward surface of the airfoil are shown in the above figures.

In Figure 12(a) it is observed that for configuration (a) the velocity profile at x = 0.65 shows inflection. The gradient $\partial U/\partial y$ seems to be quite small which indicates low wall shear stress and consequently near onset of separation. For (b) considerable momentum deficit is seen at (x/c) = 0.65 as compared to that at (x/c) = 0.1, however the flow still shows a fuller velocity profile. There is not much difference in the BL profiles of (c) and (d) apart from the fact that (d) shows slightly higher values of velocity all through the thickness of the BL as compared to (c). The velocity profiles of (c) and (d) show clear contribution of the moving surface in enhancing boundary layer momentum content and consequently the robustness of the flow.

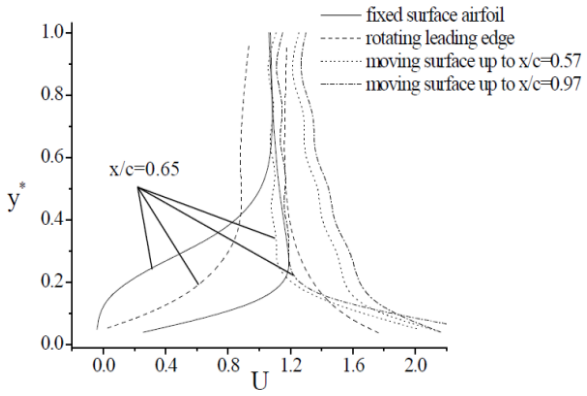

Figure 12(a). Time averaged boundary layer velocity distribution for fixed surface and moving surface airfoil at α = 10°

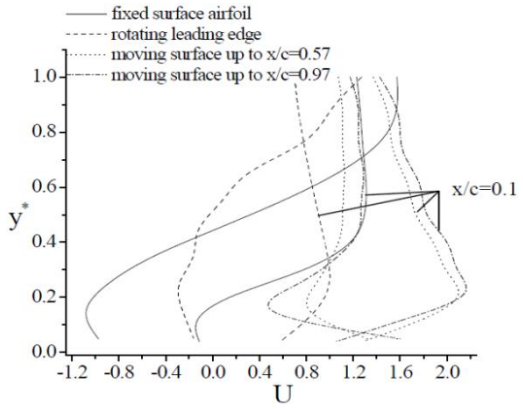

Figure 12(b). Time averaged boundary layer velocity distribution for fixed surface and moving surface airfoil at α = 30°

Figure 12(b) shows that for (a) flow reversal has already initiated at (x/c) = 0.1 which becomes more adverse at (x/c) = 0.65. For (b) the flow reversal is seen at (x/c) = 0.65. Regions of low momentum are seen in the velocity profiles of (c) and (d). However, there is no indication of flow separation in these two cases.

In Figure 13 time averaged surface pressure distribution at α = 20° is shown for configurations (a), (c) and (d). It is observed that the enclosed area within the curve for (a) is well exceeded by those of (c) and (d), which indicates that (c) and (d) produces much higher lift at this angle of attack compared to (a). It is to be noted that two small kinks are observed on the leeward surface in the case of (c) and (d) at (x/c) = 0.57 and 0.97 respectively because of the abrupt change of no slip boundary condition across the end point of the moving surface. Such kink is however weakly visible where the moving surface starts at the leading edge because of very highly accelerated flow due to combined effect of moving boundary along with nose radius.

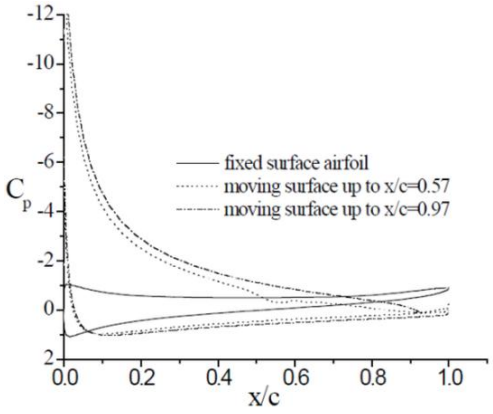

Figure 13: Time-averaged surface pressure distribution at α = 20°

The coefficient of lift and drag variations with varying angle of attack for various configurations are shown in Figures 14 and 15 respectively. It is observed from the lift coefficient distribution that (c) and (d) have comparable performance up to α = 10°. Performance of (b) is superior to (a) but inferior to the above two. Configurations (c) and (d) out-perform the others substantially above 10° angle of attack, with (d) remaining the most superior consistently. Negative drag is observed for (d). This is because the moving boundary creates a strong suction effect which has a component action along the forward direction leading which negates the drag and produces a weak propelling force. For the same reason (c) has very small drag coefficient up to α = 10°. There is sharp increase in drag coefficient for (d) beyond α = 30°. For (b) drag remains positive over entire angles of attack range and grows more gradually with increase in angles of attack, however, it is lower than that of fixed surface airfoil.

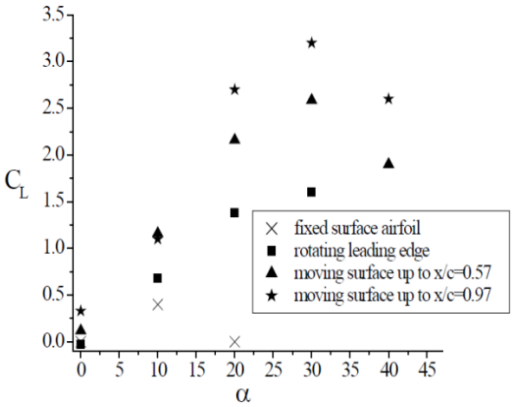

Figure 14: Coefficient of lift variation with angles of attack

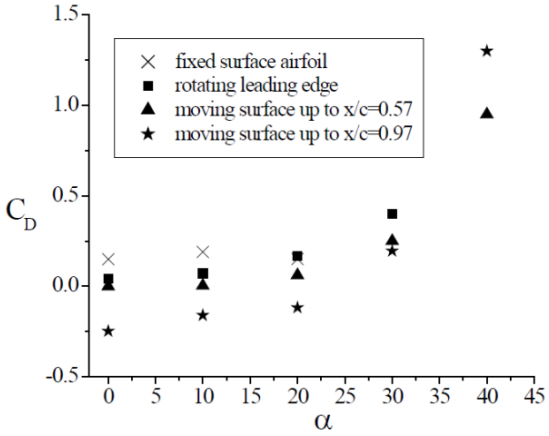

Figure 15: Coefficient of drag variation with angles of attack

IV. CONCLUSIONS

In this paper a numerical study was performed to investigate the consequence of MSBL control on the aerodynamic performance of the airfoil NACA 0012 at ultra-low Reynolds number. Not much research is reported in literature on aerodynamic effect of moving surface applied over extensive lengths of the airfoil surface. This was one of the main focus of the present study. Most of the flow simulations in this study were confined to *Re* = 100. The angle of attack was varied from 0° - 40°. A 2-d incompressible unstructured grid based on Navier Stokes solver 'CFRUNS' was used for conducting the numerical study, (Harichandan and Roy [2010]). The solver's capabilities were tested adequately before applying it to the present problem for fixed and moving boundary cases. Moving surface was applied at three different portions on the airfoil surface for conducting the present study. All the moving surface configurations showed improvement of aerodynamic performance of the airfoil through enhancement of lift, reduction of drag etc. The configuration with the largest extent of moving surface, i.e., from the leading edge to (x/c) = 0.97 has better performance in terms of lift amplification. It also leads to maximum drag reduction and leads to negative drag at low angles of attack. However, on a practical configuration it may be difficult to install such a mechanism because a major portion of the trailing edge of a lifting surface needs to be deflected for control purposes and having a moving surface on a deflecting component would be very complex. From that point of view the configuration with moving surface from leading edge to (x/c) = 0.57 would be a better choice with not much sacrifice on the performance of the airfoil within the operating angle of attack range that was studied. A reasonably detailed aerodynamic analysis of the various configurations were performed including study of lift and drag characteristics, surface pressure and shear stress, streamline patterns, boundary layer velocity distribution etc. The study suggests that moving surface boundary layer control would be an effective flow control mechanism at ultra-low Reynolds numbers

ACKNOWLEDGMENT

It is optional. The preferred spelling of the word "acknowledgment" in American English is without an "e" after the "g." Use the singular heading even if you have many acknowledgments. Avoid expressions such as "One of us (S.B.A.) would like to thank ... ." Instead, write "F. A. Author thanks " *Sponsor and financial support acknowledgments are placed in the unnumbered footnote on the first page*.

REFERENCES

1. Johnson, W.S., Tennant, J.S. and Stamps, R.E., 1975.Leading edge rotating cylinder for boundary-layer control on lifting surfaces.AIAA Journal of Hydronautics, 9, 76–78.
2. Moktarian, F. and Modi, V.J., 1988. Fluid dynamics of airfoils with moving surface boundary-layer control**,** Journal of Aircraft, 25(2), 163-169
3. Modi, V.J. and Mokhtarian, F., 1990.Effect of moving surfaces on the airfoil boundary layer control. Journal of Aircraft, 27, 42-50.
4. Hassan, A.A. and Sankar, L.N., 1992. Separation control using moving surface effects-A numerical simulation**.** Journal of Aircraft, 29(1), 131-139.
5. Kubo, Y., Modi, V.J., Yasuda, H. and Kato,K., 1992.On the suppression of aerodynamic instability through the moving surface boundary-layer control.Journal of Wind Engineering and Industrial Aerodynamics, 41,205–216.
6. Modi, V.J., Munshi, S.R., Mokhtarian, F., Bandyopadhyay, G., Yokomizo, T., 1994.Multielement airfoils with moving surface boundary layer control: Wind tunnel, numerical and flow visualisation studies.19th ICAS Congress/ AIAA Aircraft System Conference, 1-24.
7. Modi, V., 1997. Moving surface boundary-layer control: a review. Journal of Fluids and Structures, 11, 627-663.
8. Azuma, D. and Nakamura, Y., 2002. Lift enhancement of a thick delta wing using rotational leading edges. AIAA-Paper, 2002-847.
9. Harichandan, A.B. and Roy, A., 2010. Numerical investigation of low Reynolds number flow past two and three circular cylinders using unstructured grid CFR scheme. International J. of Heat and Fluid Flow, 31, 154–171.
10. Harichandan, A.B. and Roy, A., 2012. Numerical investigation of flow past single and tandem cylindrical bodies in the vicinity of a plane wall. Journal of Fluids and Structures, 33, 19–43.
11. Roy, A. and Bandyopadhyay, G., 2006.A finite volume method for viscous incompressible flows using a Consistent Flux Reconstruction Scheme. International Journal for Numerical Methods in Fluids, 52(3), 237-354.
12. Ding H, Shu C, Yeo K. S, and Xu D., 2007. Numerical simulation of flows around two circular cylinders by mesh-free least square-based finite difference methods.
13. Meneghini JR, Saltara F, Siqueira CLR and Ferrari Jr JA., 2001. Numerical simulation of flow interference between two circular cylinders in tandem and side-by-side arrangement. Journal of Fluids and Structures, 15,327-350.
14. Braza M, Chassaing P, and Ha Minh H., 1986. Numerical study and physical analysis of the pressure and velocity fields in the near wake of a circular cylinder. Journal of Fluid Mechanics, 163, 79-130.
15. Tritton D.J., 1959. Experiments on the flow past a circular cylinder at low Reynolds numbers. Journal of Fluid Mechanics, 6, 547.
16. Wiesenberger VC., 1921. Neuere festellungen uber die Gesetze des Flussigkeits und uftwiderstands. Physik. Z.22, 231.
17. Huang, R.F., Wu, J.Y., Jeng, J.H. and Chen, R.C., 2001.Surface flow and vortex shedding of an impulsively started wing. Journal of Fluid Mechanics, 441, 265-292.
18. Ingham, D.B., 1983.Steady flow past a rotating cylinder. Computers and Fluids, 11(4), 351-366.
19. Supradeepan, K., and Roy, A., 2015. Low Reynolds number flow characteristics for two side by side rotating cylinders. ASME Journal of Fluids Engineering, 137(10) 101204.

AUTHORS PROFILE

Mr. Yagnesh Joshi is an Assistant Professor at Government Engineering Gollege (GEC) at Rajkot having ten years of teaching experience. He has completed Maters in Mechanical engineering and currently pursuing his Postgraduate degree. He is highly skilled at engineering graphics, engineering thermodynamics, fluid mechanics, IC engines, automobile engineering, heat transfer and computational fluid dynamics. He is also working on experimental aerodynamic using Subsonic Wind Tunnel and water tunnel. He is also a professional member of IEI India. He has a professional teaching experience of 10 years and 1.25 years of industrial experience. He has been a C certificate holder in NCC.

Mr. Ankit Kumar, Researcher in the Department of Aerospace Engineering at KIIT deemed to be University at Bhubaneswar, has been relentlessly working on experimental and numerical aerodynamics. His keen interest in Computational Fluid Dynamics prompts him to work on novel ideas in the field of Aerodynamics. He has also been working on shock waves and ultra-low Reynolds number flow. He also works on NI LabVIEW, SolidWorks and has also been doing research on Aero-engines and designing of self stabilizing airplanes, robotics and rotary aerial vehicles. He has a great interest in cosmology and has been working on black holes for a long time.

Dr. Arnab Roy, Associate Professor in the Department of Aerospace Engineering at IIT Kharagpur, has been a skilled researcher in the field of Computational Fluid Dynamics, Multiphase Flow, Low Reynolds number Aerodynamics, DNS and LES and Flapping Wing Aerodynamics. He has also been working on Aerodynamic study of high speed train configurations, multiphase flow simulations in hybrid rocket combustors and Chaff Cloud Aerodynamics. He is currently working as Moderator for Institute Patent Portal and Co-Professor-In-Charge for Academy of Classical and Folk Arts. He is currently involved in a design, analysis and development of Nozzle Protection System for Sea Level Testing of CE20 Engine with A/R 100 for ISRO Propulsion Complex.

Dr. Atal Bihari Harichandan, Associate Professor in the Department of Aerospace Engineering at KIIT deemed to be University, has keen interests on Computational Fluid Dynamics, Low Reynolds number Aerodynamics, Combustion, electronic cooling and gas dispersion modeling. He is a respected member of American Society for Mechanical Engineers (ASME). He has also been working on Gas Turbine, Jet propulsion and Experimental Aerodynamics. He has also developed incompressible finite volume laminar Navier-Stokes solvers based on 2-D unstructured grid named CFRUNS. He has also worked on axial flow turbines using MATLAB. He has also been working on shock waves and low Reynolds number flow in Mars atmosphere.